Electronic Supplementary Information

Boosted photoredox capability of visible-active P-doped C_3N_4 with efficient harvesting of electron-hole pairs

Asmita Dileep Gaonkar, [a] Shraddha Paniya, [a] Srinivasu Kancharlapalli,[b,c] and Kiran Vankayala [a,*]

[a] Functional Materials for Electrochemistry and Solar energy (FunMatES) Group, Energy and Environmental Chemistry Lab, Department of Chemistry, Birla Institute of Technology and Science (BITS), Pilani, K K Birla Goa Campus, Goa, 403726.
[*]Email: kiranv@goa.bits-pilani.ac.in; kiran2cu@gmail.com
[b] Chemistry Division, Bhabha Atomic Research Centre, Mumbai, India, Homi Bhabha National Institute, Anushaktinagar, Mumbai, India

[c] Homi Bhabha National Institute, Anushaktinagar, Mumbai, India

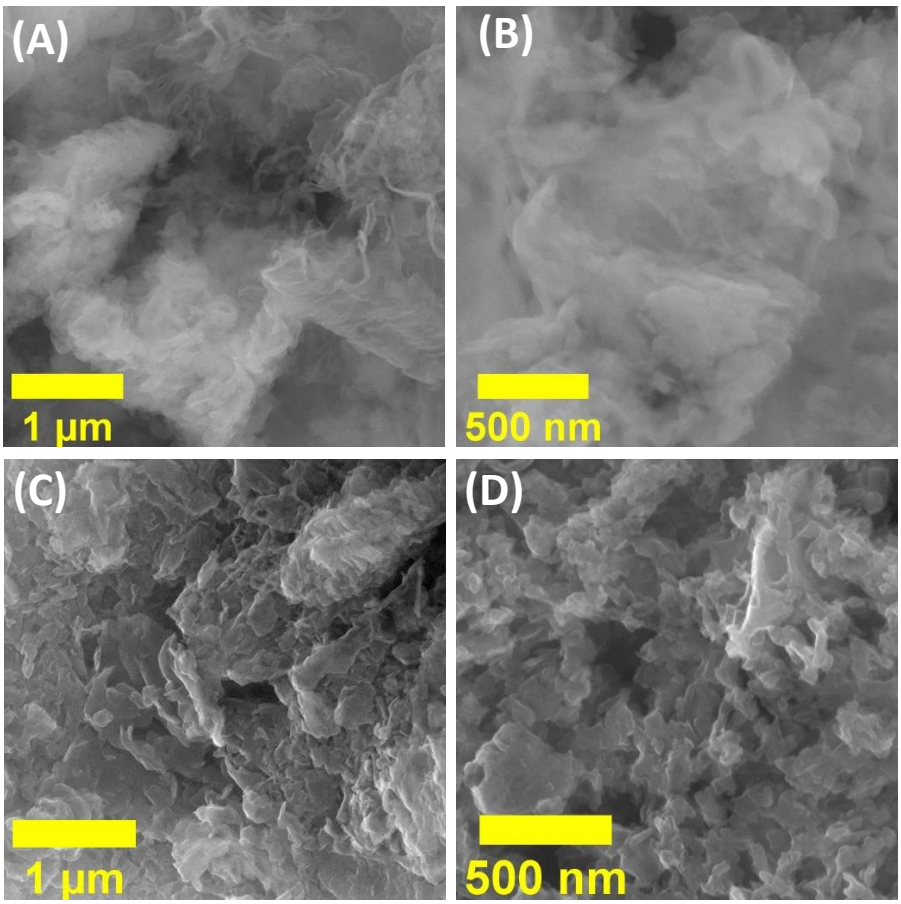

Fig. S1. FESEM images of CN-105P (A & B) and CN-315P (C & D) recorded under different magnifications.

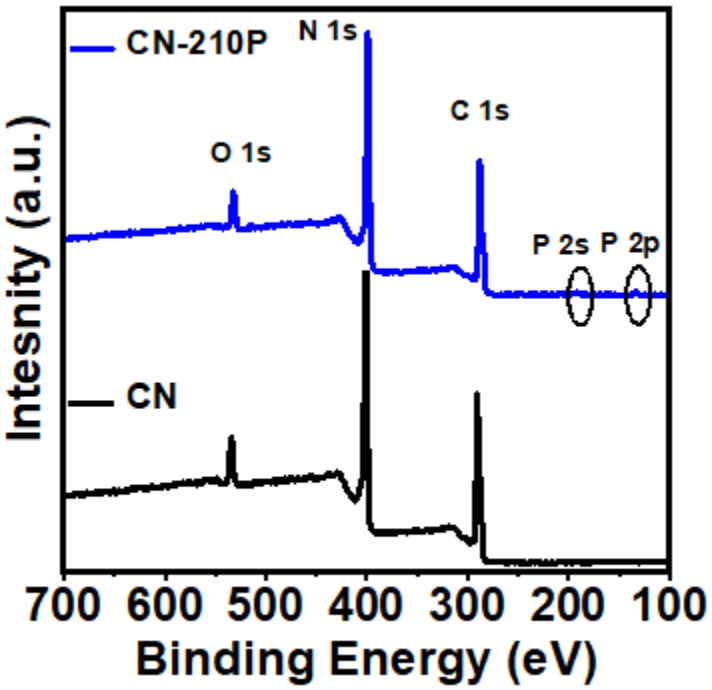

Fig. S2. XPS survey spectra of CN and CN-210P.

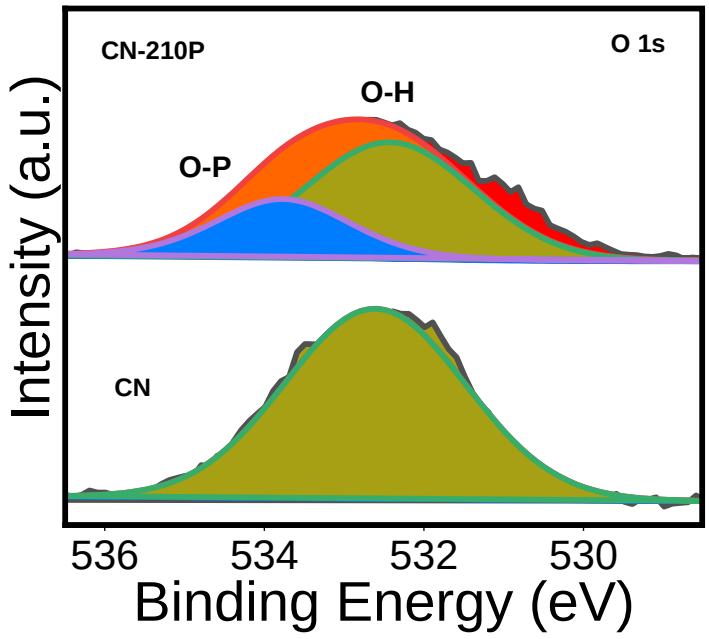

Fig. S3. XPS spectra corresponding to O1s core level for CN and CN-210P.

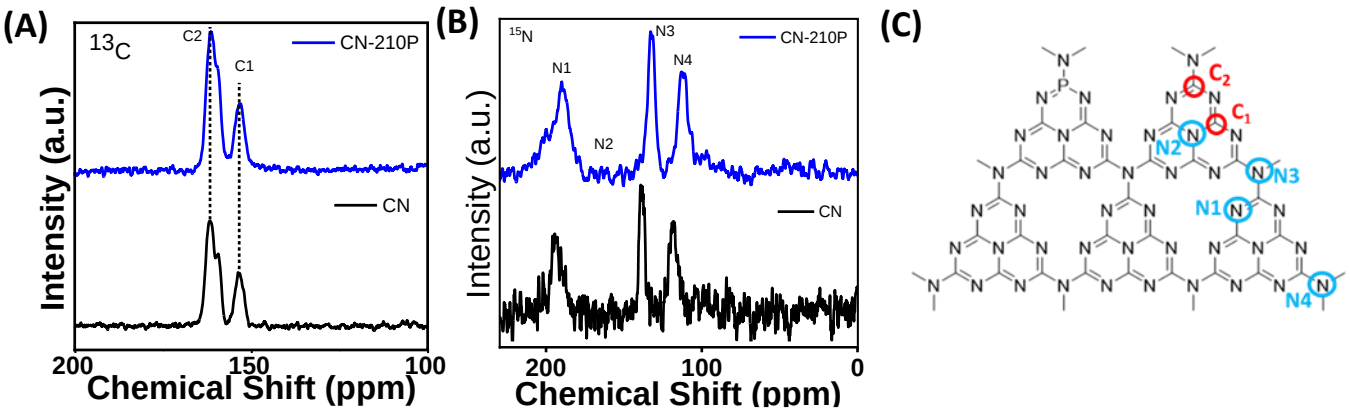

Fig. S4. CP-MAS SSNMR (A)^{13}C spectra and (B) ^{15}N spectra of CN and CN-210P. (C) Schematic representation of g-C_3N_4 framework depicting different types of C and N atoms.

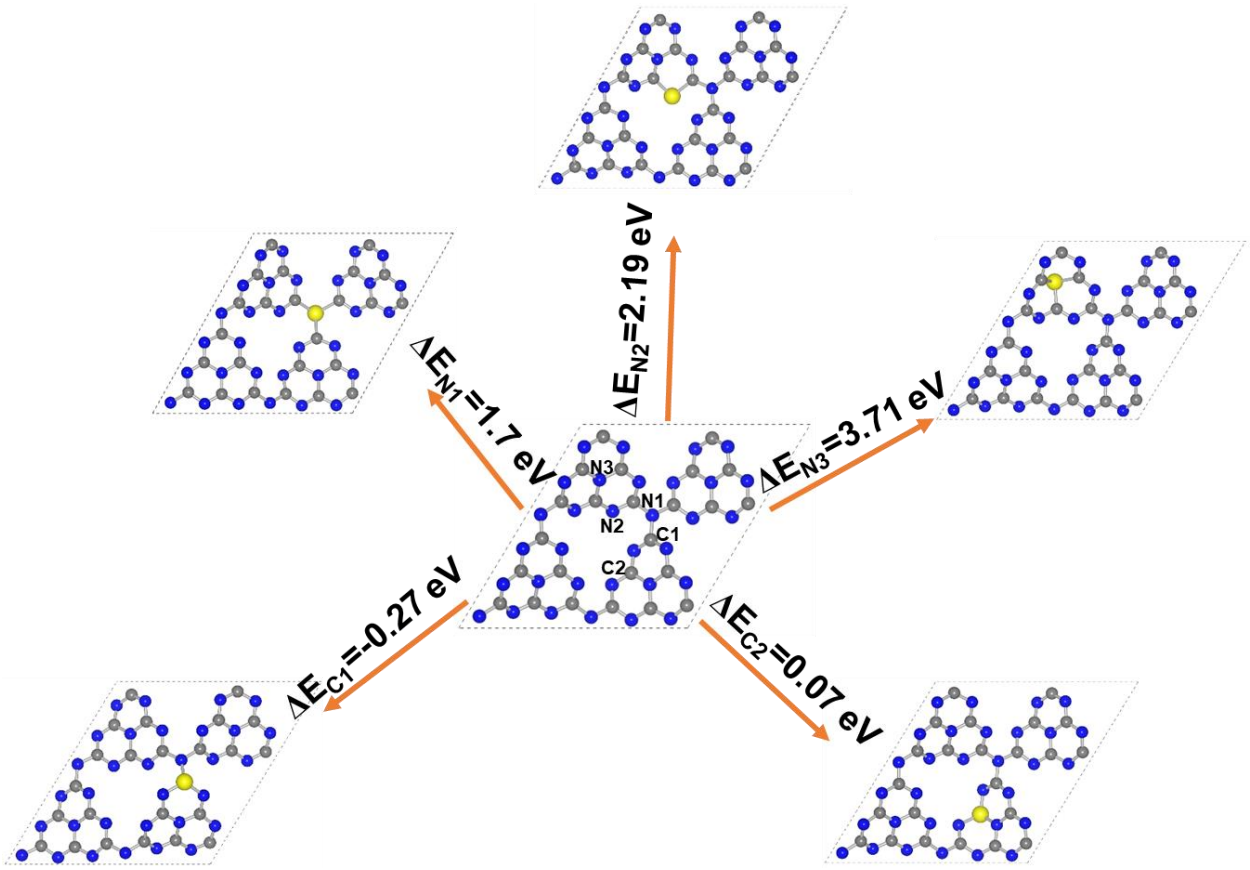

Fig. S5. Optimized structure of the 2 x 2 x 1 super cell of CN and its P-doped systems at different possible sites with the corresponding formation energies.

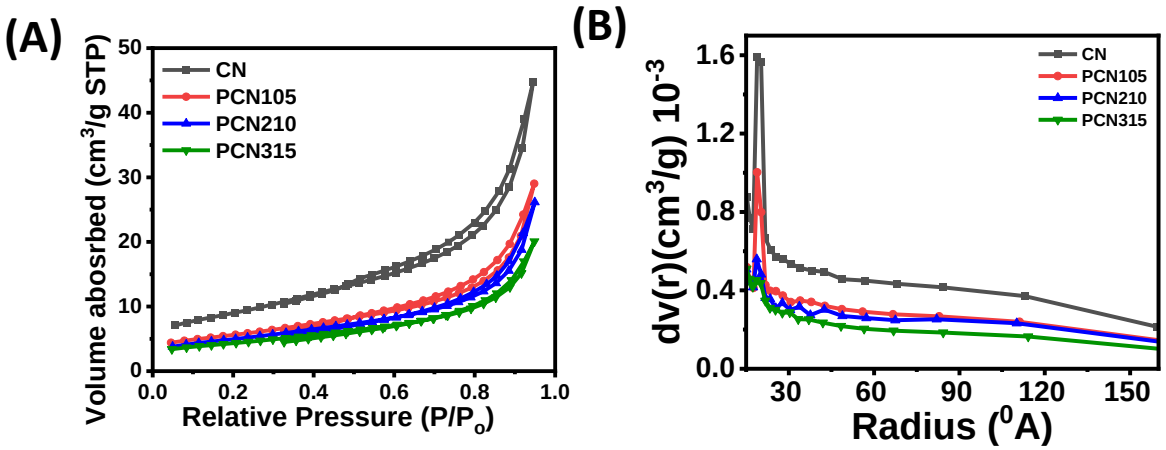

Fig. S6. (A) BET N_2 adsorption-desorption isotherms, (B) Pore size distribution of CN and CN-xP respectively.

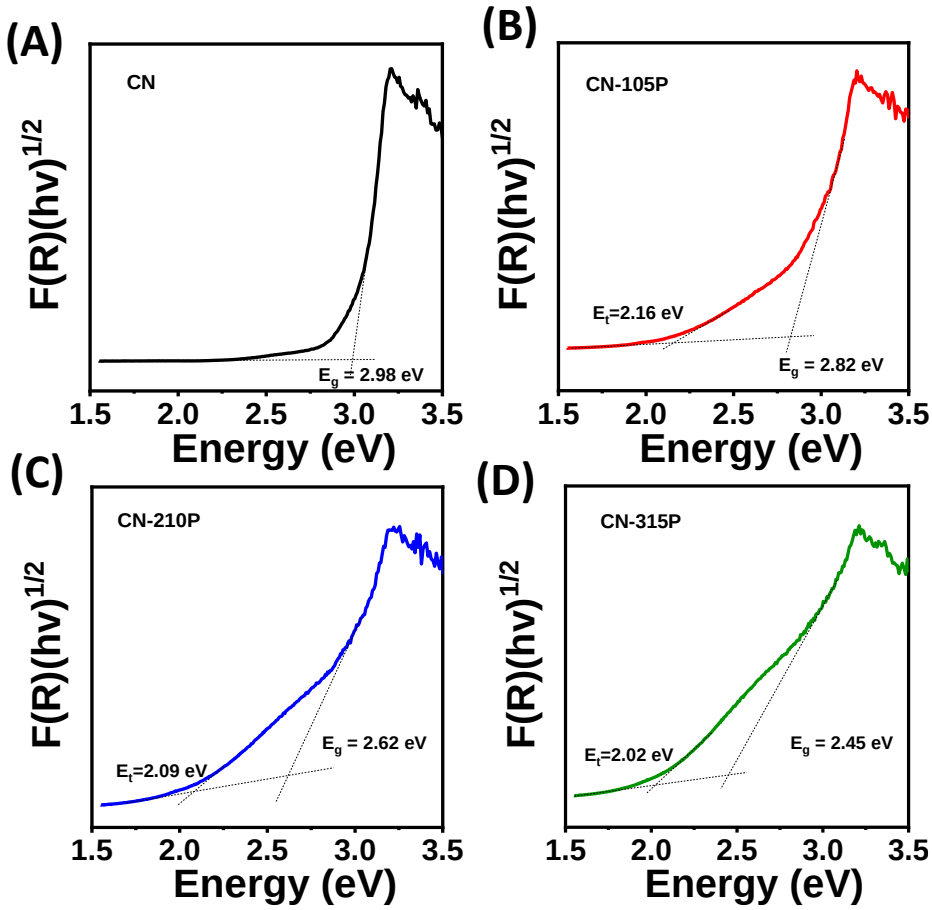

Fig. S7. Tauc Plot of (a) CN, (b) CN-105P, (c) CN-210P and (d) CN-315P.

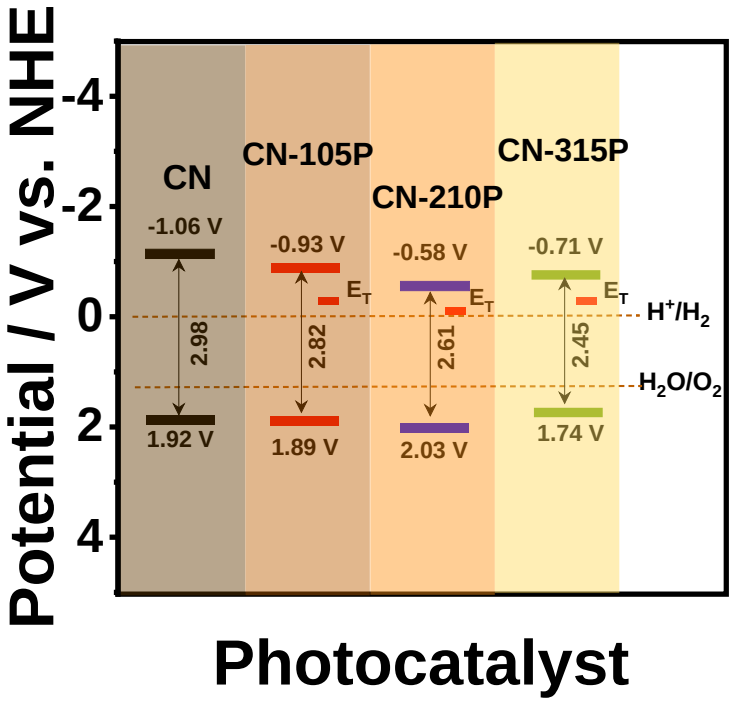

Fig. S8. The valence band (VB) and conduction band (CB) positions estimated from XPS VB spectra and UV-Vis DRS data.

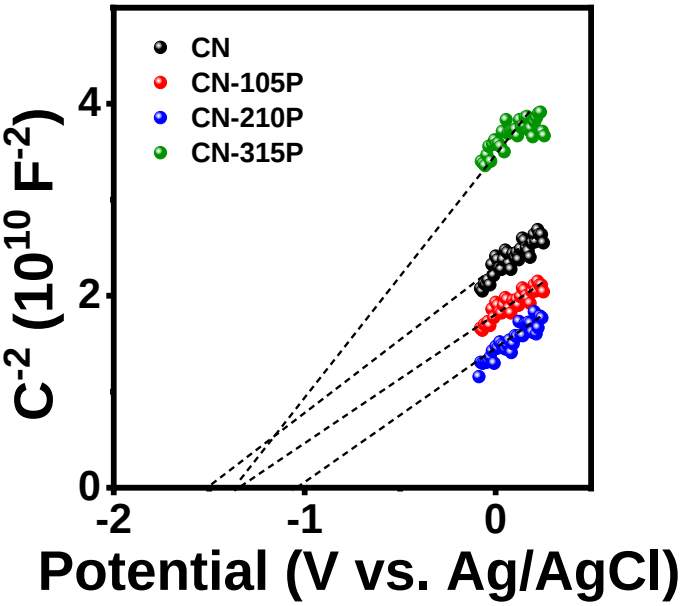

Fig. S9. Mott-Schottky plots of undoped and doped CN samples measured in 0.1 M Na_2SO_4 (pH= 6.8) at 1000 Hz.

The flat band potential of CN and CN-xP were determined from the Mott-Schottky (M-S) measurements. The positive slope of the linear plot of M-S plot suggests that prepared samples are n-type semiconductors, as expected. The position of conduction band (CB) E_{CB} vs. RHE for all samples was calculated using the following equation.[1]

$$E_{CB}(RHE) = E_{Fb} + 0.059pH + E^{0}{}_{Ag/AgCl}$$

where $E^{o}_{Ag/AgCl}$ = 0.198 V vs. NHE, E_{Fb} is flat band potential obtained from Fig. S7 and pH of the electrolyte used was 6.8.

The conduction band minimum (CBM) of n-type semiconductors is assumed to be present at 0.1 V more negative than $E_{fb.}$[1] Subsequently, the obtained E_{CB} vs. RHE values are converted into E_{CB} vs. NHE scale.

The calculated E_{CB} (vs. NHE) values are given in Table S4.

According to the below equation, the position of valence band E_{VB} (vs. NHE) was determined using band gap value obtained from UV-DRS data and E_{CB} (vs. NHE) value obtained from M-S data.

$$E_{VB(NHE)} = E_g + E_{CB(NHE)}$$

where E_g is the band gap of the semiconductor, E_{VB} and E_{CB} are valence and conduction band positions respectively.

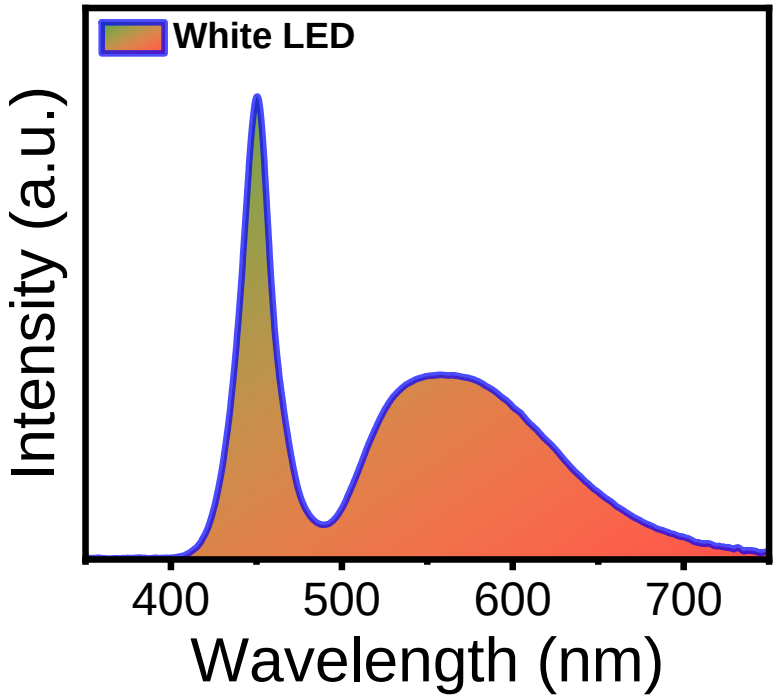

Fig. S10. Spectral output of the white LED used for photocatalysis in the present study.

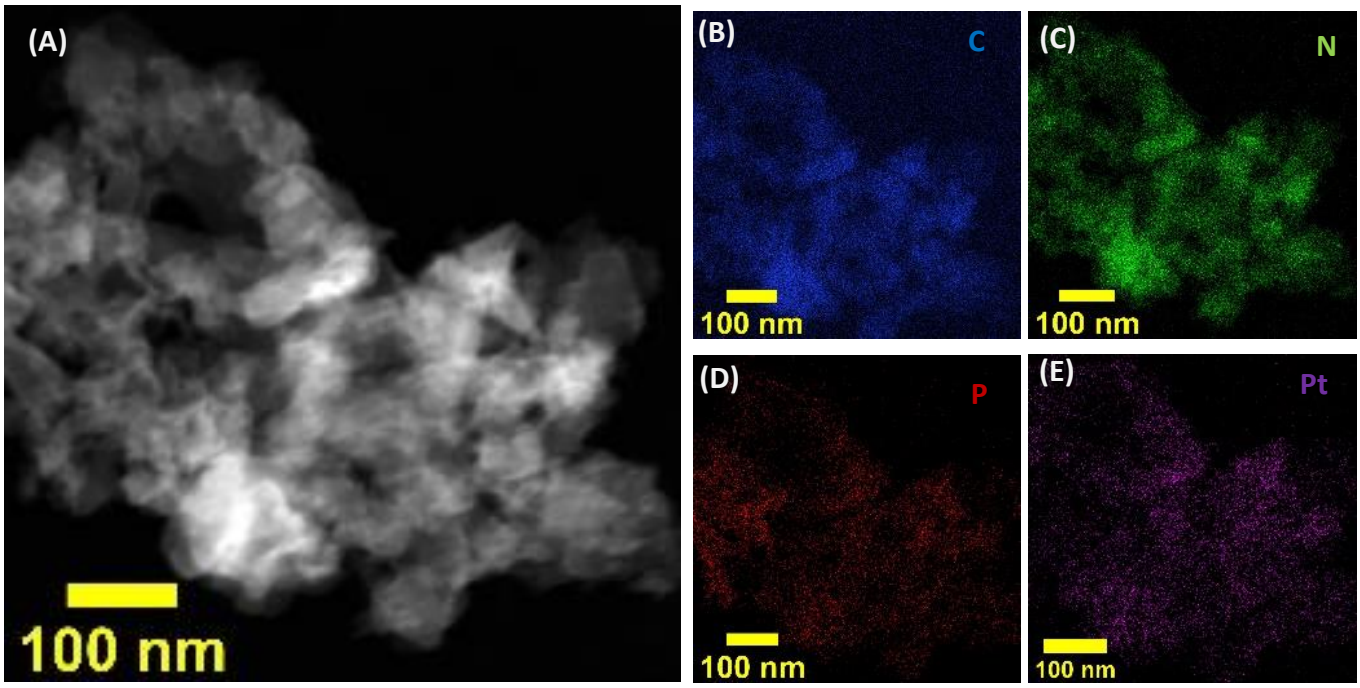

Fig. S11. (A) STEM-HAADF images of CN-210P modified with Pt co-catalysts. (B)-(E) STEM elemental mapping corresponding to C, N, P, and Pt respectively.

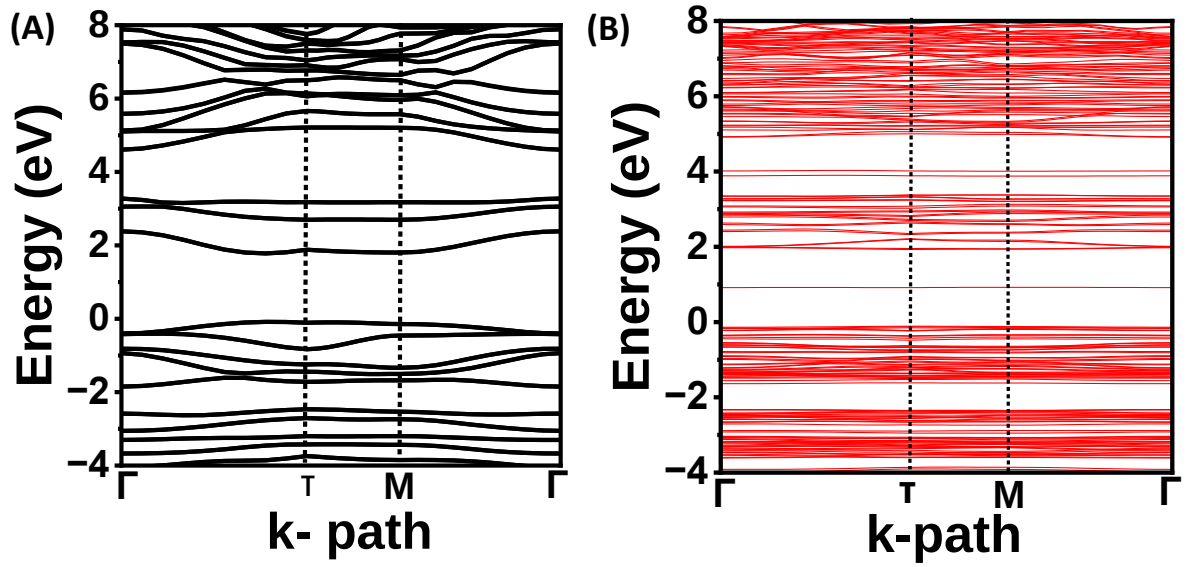

Fig. S12. Electronic band structure of (A) pure CN and (B) P-doped C_3N_4 obtained from PBE functional.

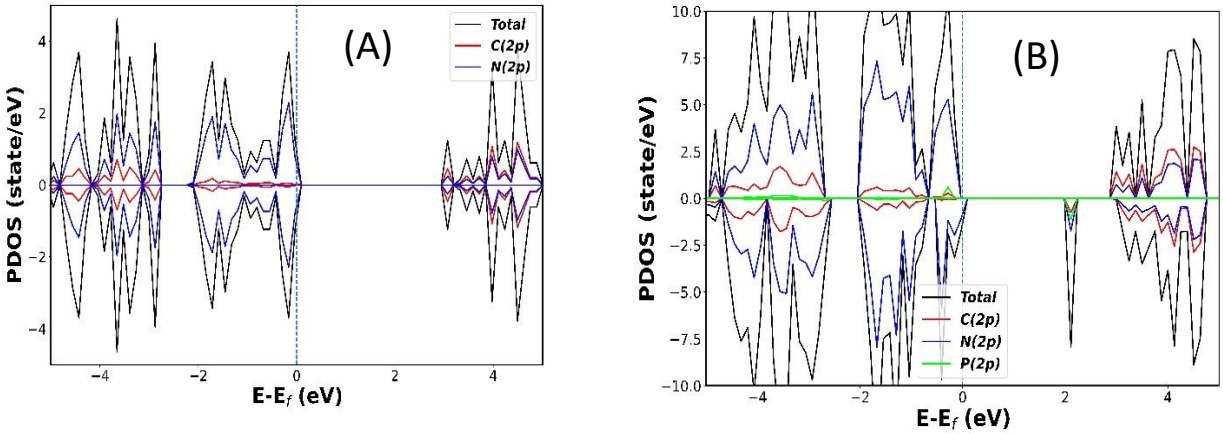

Fig. S13. Total and projected density of states of (A) CN and (B) P-doped C_3N_4.

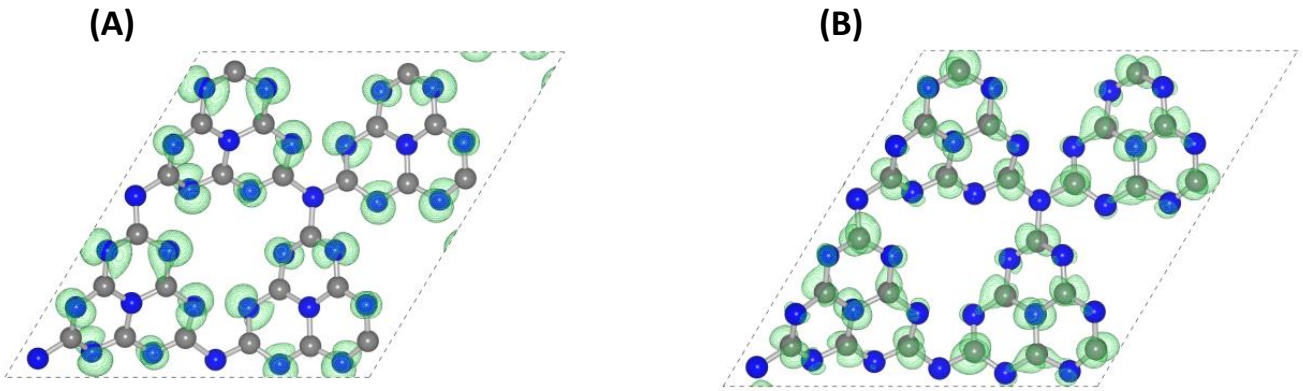

Fig. S14. Band decomposed charge density iso-surface plots of (a) valence band maxima and (b) conduction band minima of pure C_3N_4.

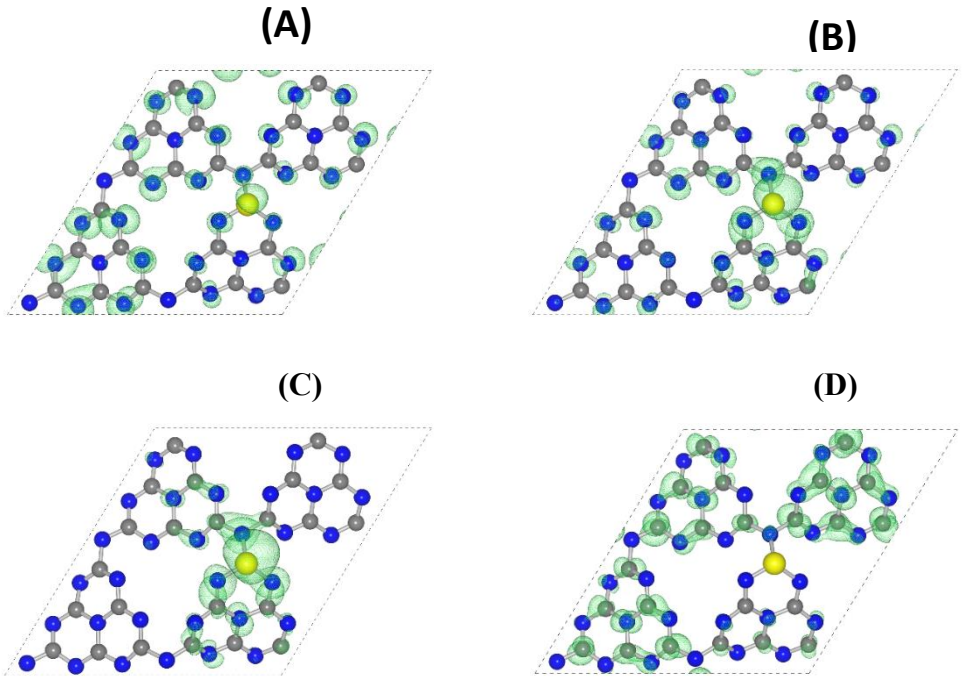

Fig. S15. Charge density iso-surface for the (A) highest fully occupied valence band (B) highest half-filled valence band (C) mid gap state and (D) conduction band minima.

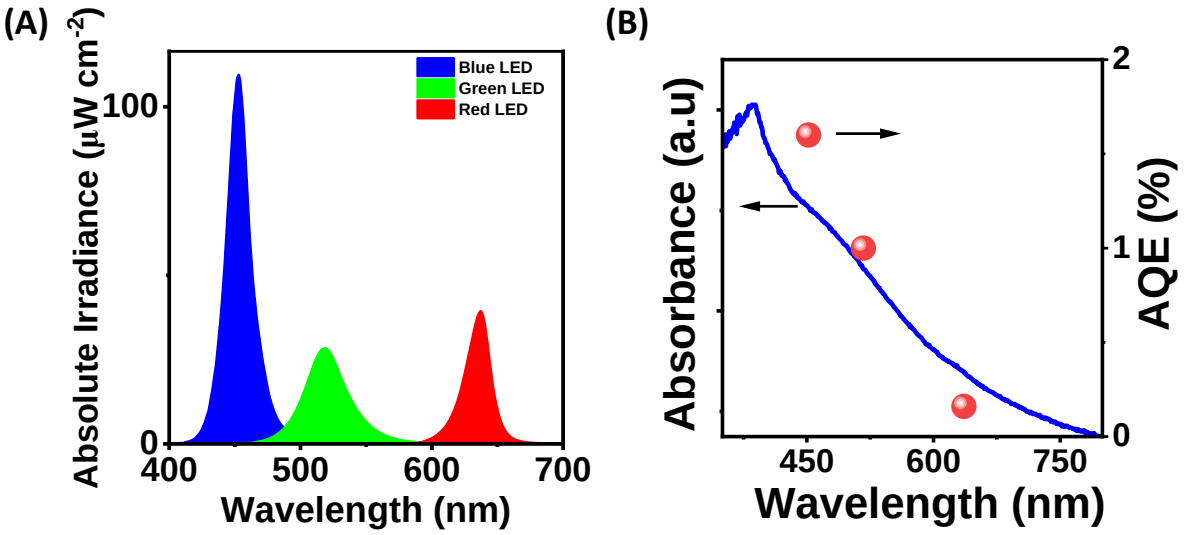

Fig. S16. (A) Spectra output of the LEDs used to determine apparent quantum efficiency (AQE), (B) UV-Vis DRS of CN-210P and AQE measured at different wavelength. Reaction condition: 10 mL water, 10 vol% TEOA, 10 mg CN-210P, Area of illumination is 3 cm^2.

Detailed calculation of AQY:

$$AQE\ (\%) = \frac{2 \times n_{H2}}{n_{photons}} \times 100 = \frac{2 \times M \times N_A \times h \times c}{P \times S \times t \times \lambda_{incident}} \times 100$$

where n_{H2} is the number of electrons transferred in H_2 evolution, $n_{photons}$ is the total number of incident photons, M is the amount of H_2 in moles, N_A is the Avogadro number, h is the Planck's constant, c is the speed of light, S is the irradiation area, P is the intensity of irradiation light, t is the photoreaction time and λ is the wavelength of incident light.

For Blue light (452 nm)

$$AQE = \frac{2\times0.0367\times10^{-6}\ mol\times6.023\times10^{23}\ mol^{-1}\times6.623\times10^{-34}JS\times3\times10^{8}ms^{-1}}{109\times10^{-6}\ Wcm^{-2}\times3\ cm^{2}\times3600\ s\times452\times10^{-9}\ m} \times 100 = 1.65\ \%$$

For Green light (517 nm)

$$AQE = \frac{2\times0.0047\times10^{-6}\ mol\times6.023\times10^{23}\ mol^{-1}\times6.623\times10^{-34}JS\times3\times10^{8}ms^{-1}}{20\times10^{-6}\ Wcm^{-2}\times3\ cm^{2}\times3600\ s\times517\times10^{-9}\ m} \times 100 = 1.00\ \%$$

For Red light (636 nm)

$$AQE = \frac{2\times0.0019\times10^{-6}\ mol\times6.023\times10^{23}\ mol^{-1}\times6.623\times10^{-34}JS\times3\times10^{8}ms^{-1}}{39\times10^{-6}\ Wcm^{-2}\times3\ cm^{2}\times3600\ s\times636\times10^{-9}\ m} \times 100 = 0.16\ \%$$

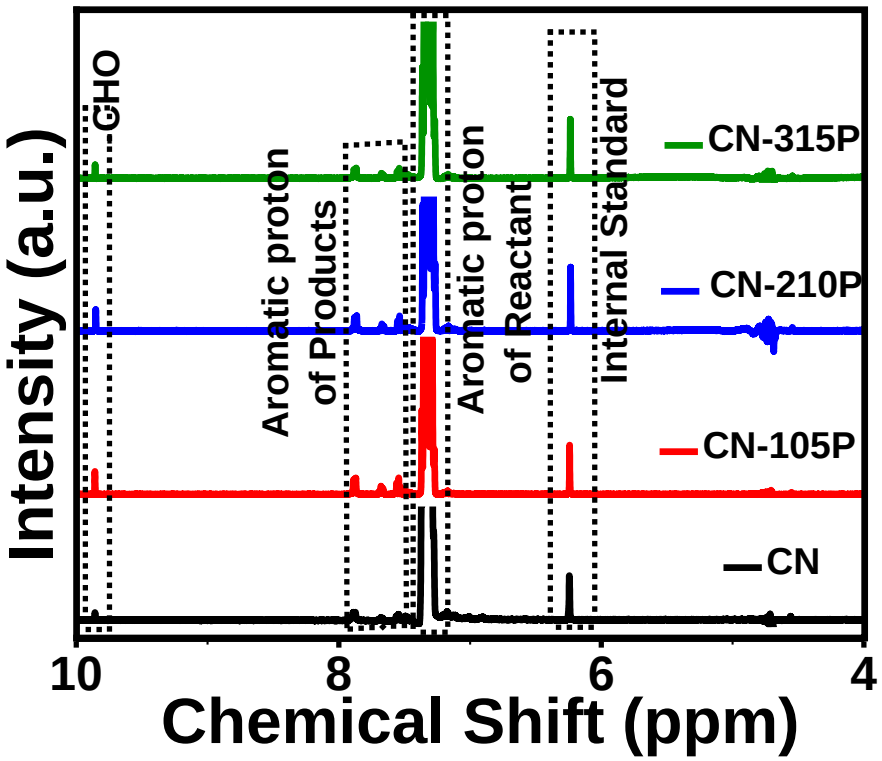

Fig. S17. ^{1}H NMR spectra of the reaction mixture obtained after 7 h. of photocatalysis carried out with undoped and CN-xP. D_2O is used as a solvent, and 1 mM Maleic acid is used as an internal standard. Reaction conditions: 10 mg Catalyst, 20 mM BA in H_2O, illumination of white LED light for 7 h.

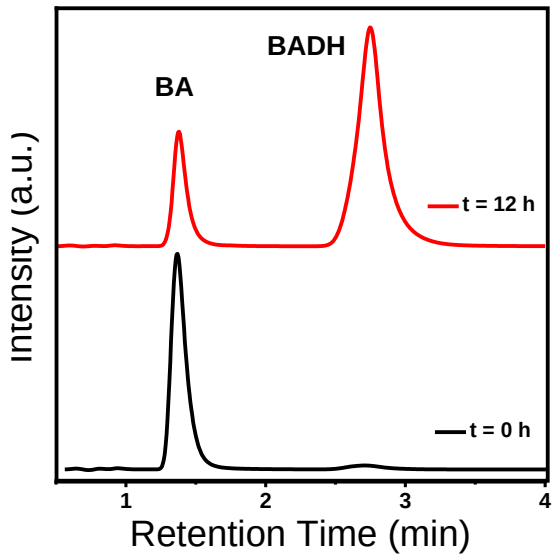

Fig. S18. LC data of the reaction mixture before and after 12 h. of the reaction, carried out using CN-210P as photocatalyst. Reaction conditions: 10 mg Catalyst, 20 mM BA in H_2O, illumination of white LED light for 12 h.

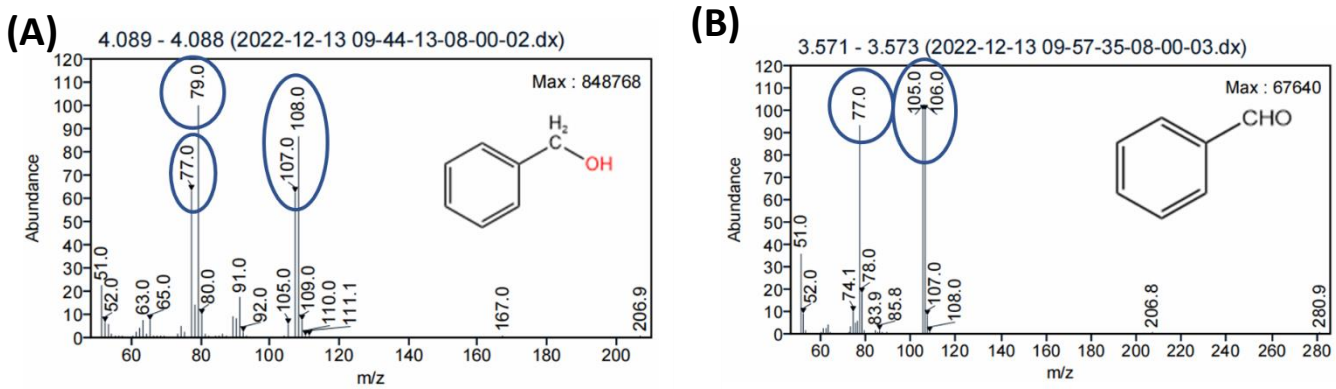

Fig. S19. (A) Mass spectra of the reaction mixture collected and extracted after illuminating the reaction mixture for 12 h. Reaction conditions: 10 mg Catalyst (CN-210P), 20 mM BA in H_2O, illumination of white LED light for 12 h.

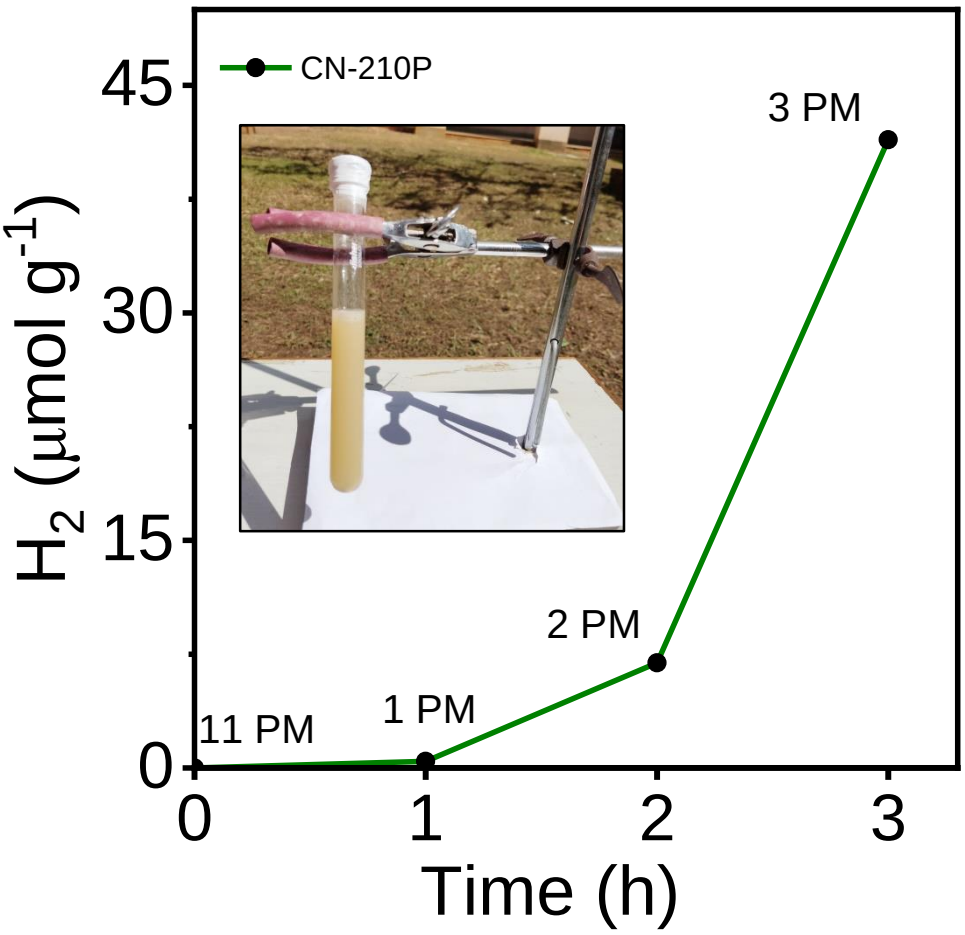

Fig. S20. Photocatalytic hydrogen evolution studies carried out under natural sunlight conditions. Inset shows picture depicting the experimental setup kept under natural sunlight. Reaction conditions: 10 mg of CN-210P, 20 mM BA in H_2O, carried out on 22nd Feb 2024 between 11-3 PM.

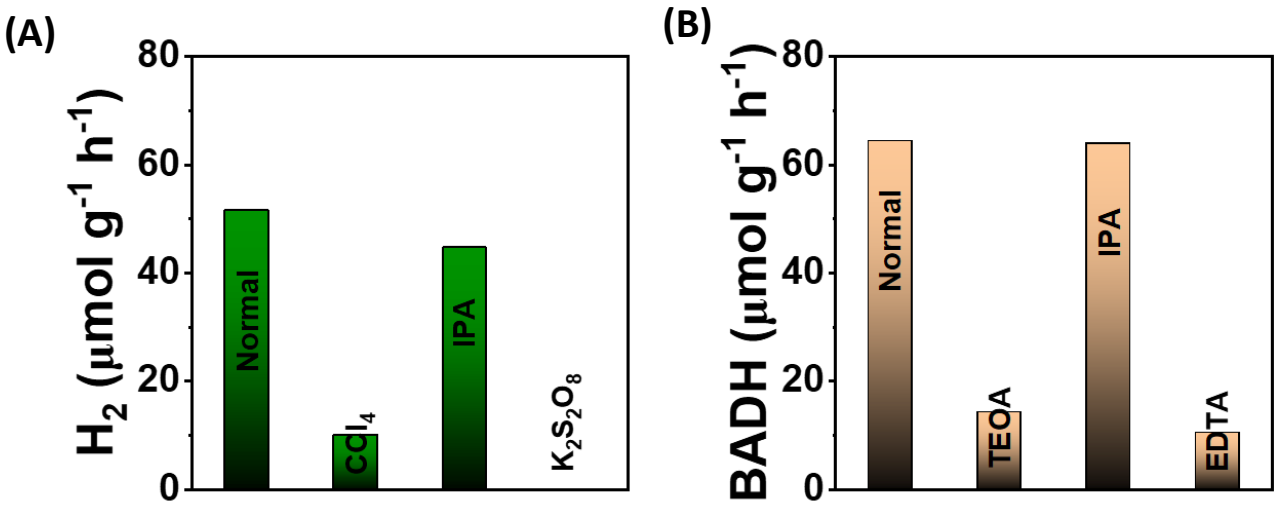

Fig. S21. Production of (A) H_2 and (B) BADH using CN-210P as photocatalyst. Normal Reaction conditions: 10 mg of CN-210P, 20 mM BA in H_2O (Normal), illumination of white LED light for 6 h. Scavenger: 40 mM (IPA or EDTA or CCl_4 or $K_2S_2O_8$ or TEOA).

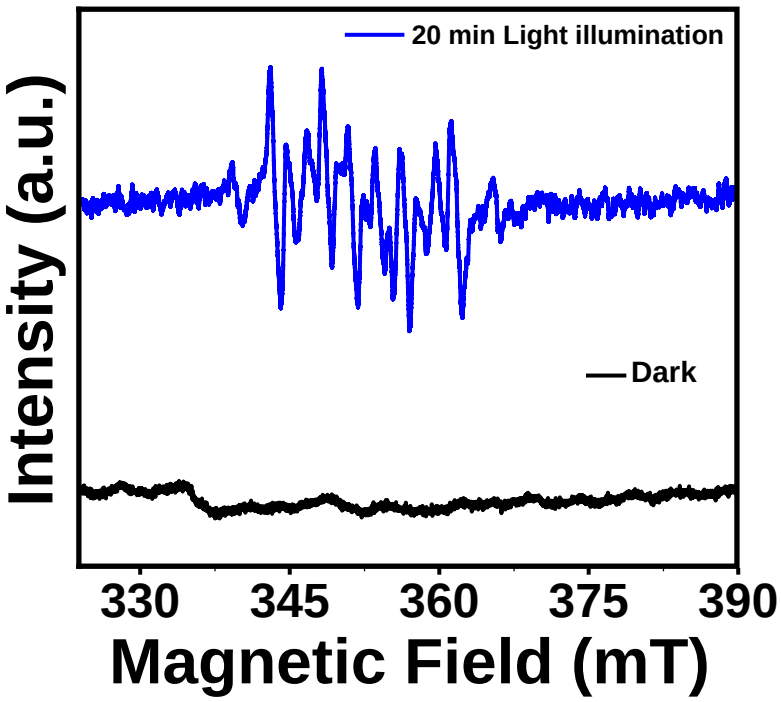

Fig. S22. ESR spectra recorded using DMPO-spin trapping agent in BA aqueous solution with or without light irradiation of light. Reaction conditions: 10 mg of CN-210P, 20 mM BA.

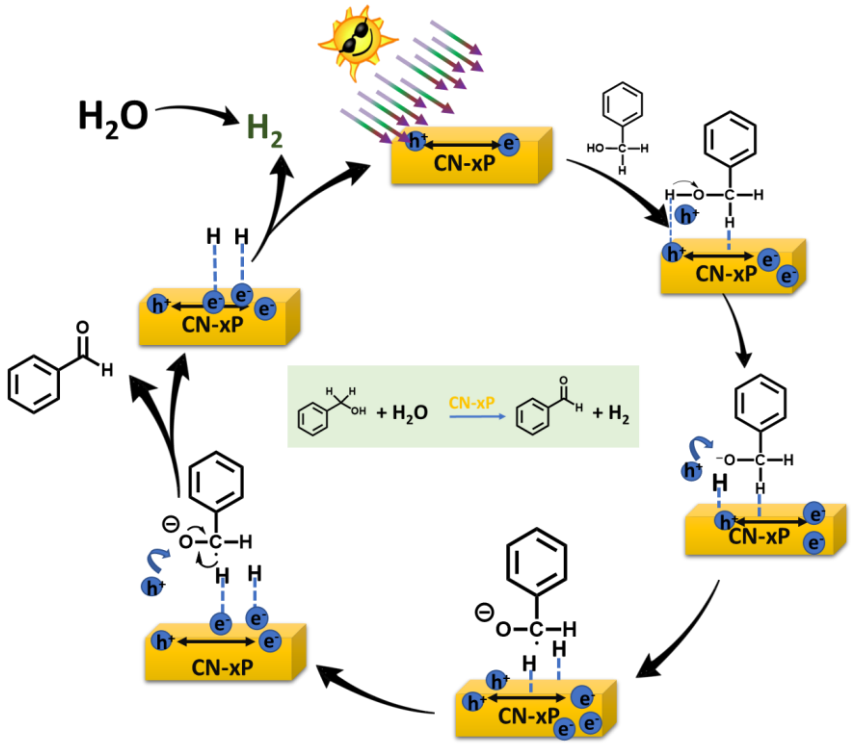

Fig. S23. Schematic representation of the proposed mechanism of the simultaneous production of BADH by selective oxidation of BA and H_2 evolution in aqueous solution under oxygen-free conditions.

To understand the benzyl alcohol oxidation reaction, the reaction schemes were simulated as

$$* + \mathrm{PhCH_2OH} \rightarrow * \mathrm{PhCH_2O} + (\mathrm{H^+} + \mathrm{e^-}) \quad (1)$$

$$* \mathrm{PhCH_2O} \rightarrow * + \mathrm{PhCHO} + (\mathrm{H^+} + \mathrm{e^-}) \quad (2)$$

Reaction energies for these reactions were calculated for both pristine and P-doped g-C_3N_4. Energy of ($H^+ + e^-$) is taken as the E(H_2)/2 at standard hydrogen electrode conditions and zero pH from the computational hydrogen electrode model which has been extensively used for simulating the redox reactions. Optimized structures of all the reaction intermediates over pure and P-doped g-C_3N_4 are reported in Fig. S24. The calculated reaction energies are plotted in Fig. S25. For the adsorption of each intermediate, different possible adsorption configurations were considered and the calculated the reaction energies are from the minimum energy structures. In both pure and P-doped systems, BA is found to interact with the catalyst surface through hydrogen bonding between the -OH group of BA and N-site of the catalyst. The calculated adsorption energy for BA is found to be -0.51 eV and -0.87 eV on pure and P-doped C_3N_4 respectively. From the adsorbed BA, dehydrogenation by removing hydrogen from -CH_2- and -OH groups are considered. In pure C_3N_4, removing the hydrogen from -CH_2- group is found to be energetically preferred while in P-doped system, -OH hydrogen removal is preferred and the corresponding structures are shown in Fig. S24. In P-doped system, after removing the hydrogen of -OH group, the O-atom of $PhCH_2O$ is chemically bonded to the P-site of the catalyst with a P-O distance of 1.575 Å while in pure system, the adsorption of PhCHOH is found to be through hydrogen bonding. Further dehydrogenation step involves the removal of H from –CH_2 group in case of P-doped C_3N_4 whereas it is from -OH group in case of pristine C_3N_4, which leads to the formation of BADH. From the free energy plots shown in Fig. S25, the overpotential for the oxidation reaction of BA to BADH is expected to be lower in P-doped C_3N_4 as compared to that in the pure C_3N_4.

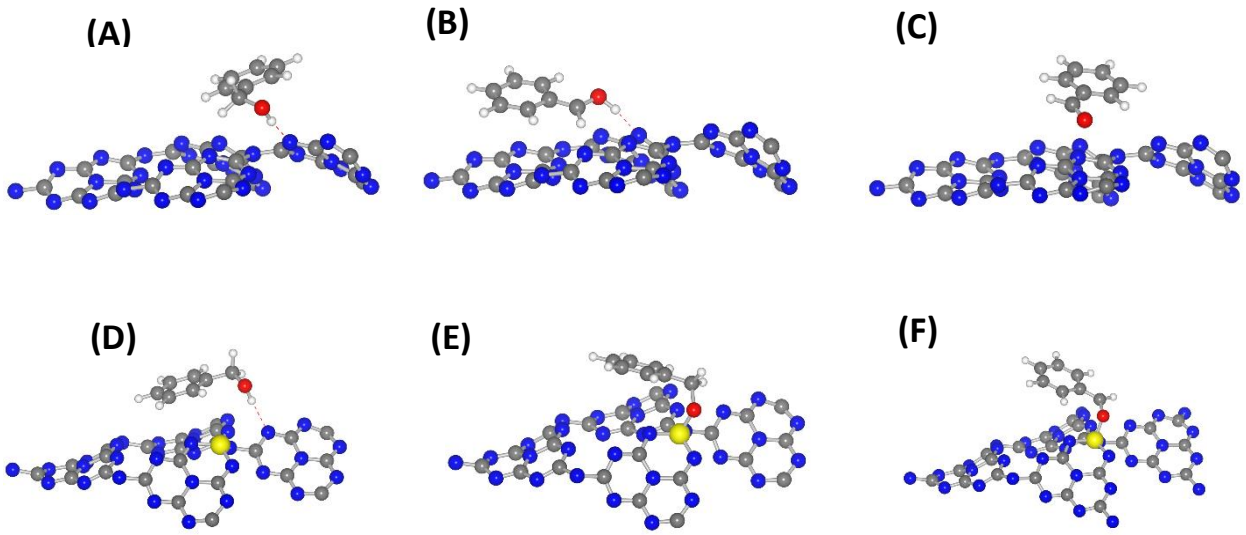

Fig. S24. Optimized structures of different reaction intermediates involved in BA oxidation over pristine C_3N_4 (A-C) and P-doped C_3N_4 (D-F).

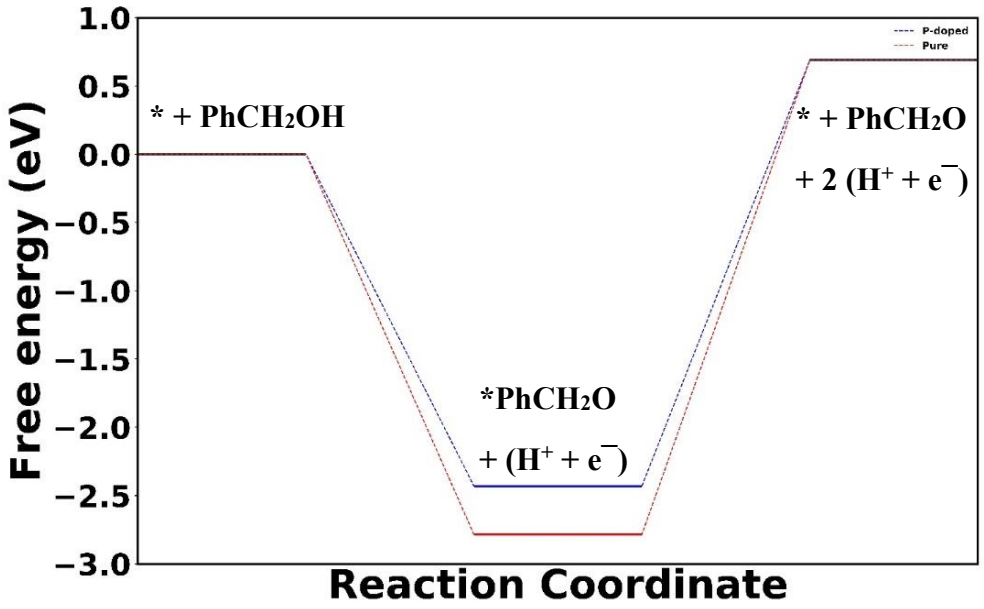

Fig. S25. Reaction energy profile for the BA oxidation over pure and P-doped g-C_3N_4.

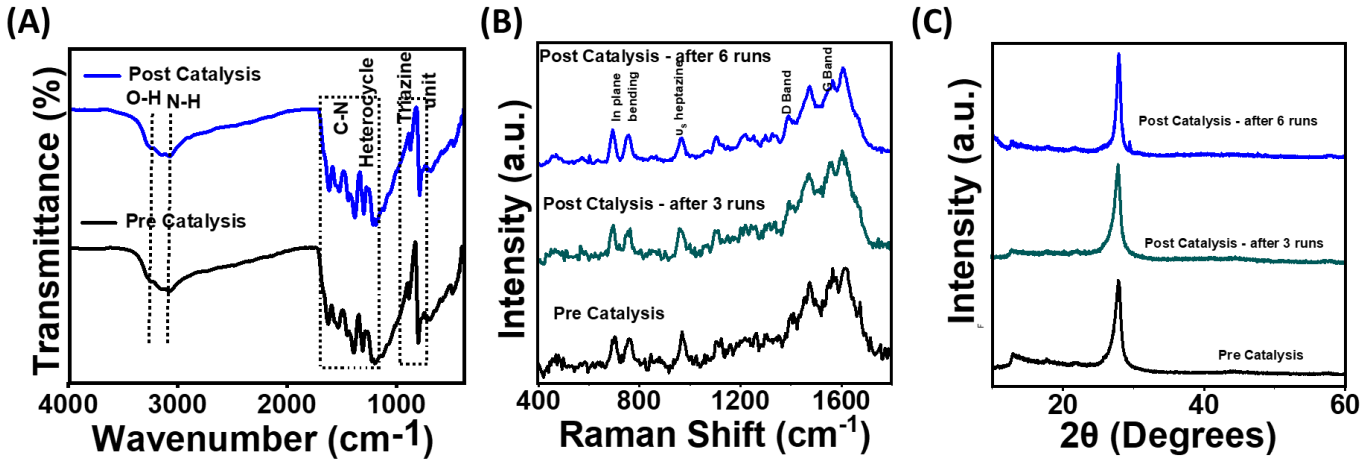

Fig. S26. (A) FTIR, (B) Raman spectra, (C) XRD patterns recorded for CN-210P before and after photocatalysis.

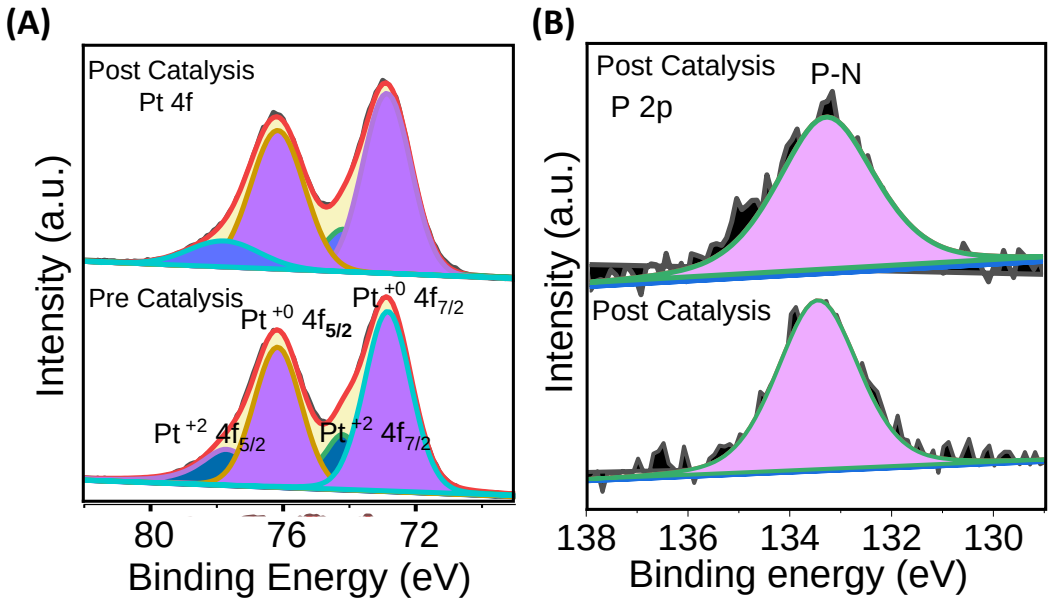

Fig. S27. XPS data of (A) Pt 4f and (B) P 2p corel levels for PtCN-210P before and after photocatalysis.

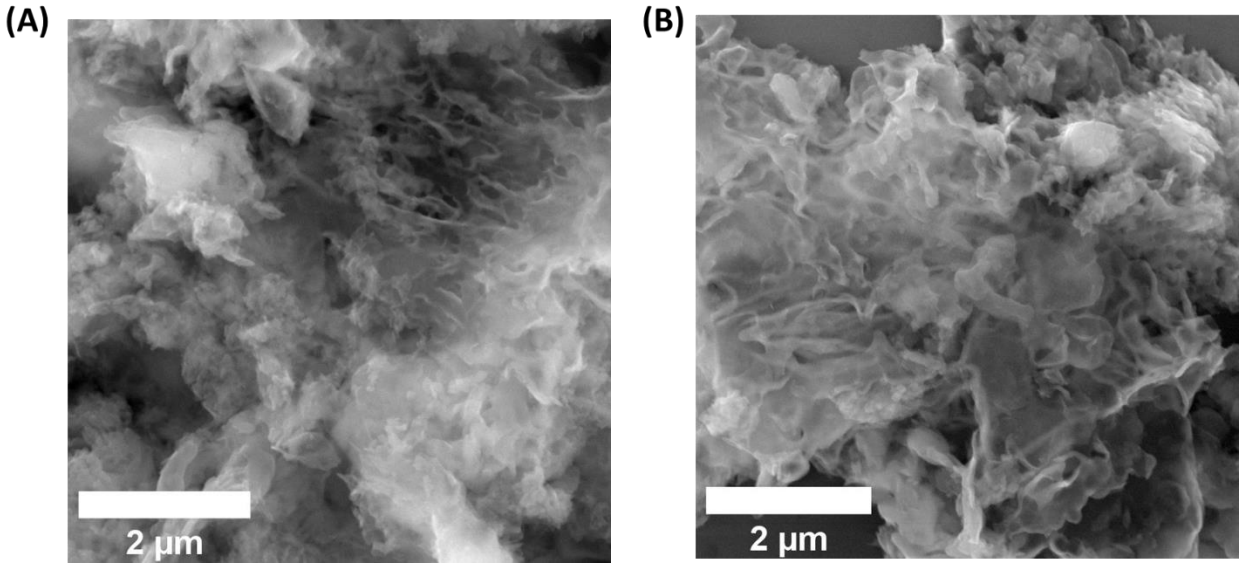

Fig. 28. FESEM images of PtCN-210P after (A) 3 runs and (B) 6 runs of photocatalysis.

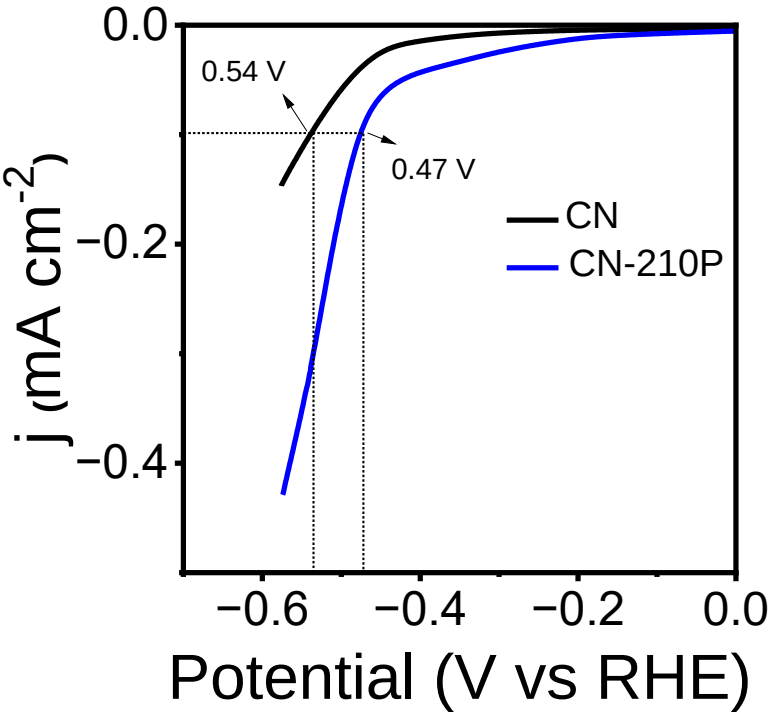

Fig. S29. LSV plot recorded using CN and CN-210P modified FTO at a scan rate of 5 mV/s in deaerated 0.1 M Na_2SO_4 (pH = 6.8).

Table S1. Comparison of I_D/I_G value of various CN-xP

Catalyst	I_D/I_G
CN	0.90
CN-105P	0.93
CN-210P	0.98
CN-315P	0.97

Table S2: Summary of the percentage elemental composition pristine and CN-xP samples obtained from CHNS analysis.

Catalyst	N Area	C Area	S Area	N %	C %	H %	Molar ratio C/N
CN	36.251	14.453	2.175	41.51	23.61	1.108	0.663
CN-105P	49.995	20.309	3.743	58.62	34.02	1.990	0.677
CN-210P	48.833	19.595	3.021	59.25	33.97	1.658	0.669
CN-315P	54.387	21.721	4.016	61.61	35.18	2.066	0.666

Table S3: Specific surface area, total pore volume and average pore size of undoped and CN-xP samples obtained from BET measurements.

Catalyst	Surface area (m^2/g)	Total pore volume (cm^3/g)	Average pore size (nm)
CN	32.834	7.124e-02	43.39
CN-105P	20.201	4.608e-02	45.62
CN-210P	18.275	4.223e-02	46.21
CN-315P	15.889	3.278e-02	41.26

Table S4: Summary of parameters for undoped and CN-xP obtained from Mott-Schottky measurements.

	E_g^*	E_{fb} (V vs. Ag/AgCl)	E_{fb} (V vs. RHE)	CB (V vs. NHE)	VB (V vs. NHE)
CN	2.98	-1.5	-0.91	-1.01	1.98
CN-105P	2.82	-1.35	-0.72	-0.82	1.99
CN-210P	2.61	-1.07	-0.47	-0.57	2.04
CN-315P	2.45	-1.28	-0.68	-0.78	1.67

* Value obtained from UV-Vis DRS.

Table S5: Summary of parameters for undoped and CN-xP obtained from VB-XPS measurements.

	E_g^*	VB-XPS	CB (V vs. NHE)	VB (V vs. NHE)
CN	2.98	2.15	-1.06	1.92
CN-105P	2.82	2.12	-0.93	1.89
CN-210P	2.61	2.26	-0.58	2.03
CN-315P	2.45	1.97	-0.71	1.74

* Value obtained from UV-Vis DRS.

Table S6. Comparison of the photocatalytic H_2 production activities of the g-C_3N_4 based systems with a sacrificial electron donor.

S. No	Catalyst	Sacrificial agent	Pt (wt. %)	H_2 (μmol g^{-1} h^{-1})	Light source	Reference
1	I-g-C_3N_4	10 vol% TEOA	3	760	300 W Xe lamp λ ≥ 420 nm	10.1002/adma.201303611
2	Br-modified g-C_3N_4	10 vol% TEOA	3	960	300 W Xe lamp	10.1016/j.apcatb.2016.03.062
3	Ultrathin g-C_3N_4 nanosheets	10 vol% TEOA	3		300 W Xe lamp	10.1039/C6RA26172H
4	Quasi-sphere g-C_3N_4	20 vol% TEOA	3	613.4	300 W Xe lamp λ ≥ 420 nm	10.1016/j.apcatb.2018.07.017
5	Ni-doped g-C_3N_4	10 vol% TEOA	3	155.71	300 W Xe lamp	10.1039/C9TA04559G
6	P-doped g-C_3N_4	10 vol% TEOA	3	506	300 W Xe lamp	10.1039/C4TA05292G
7	P-doped g-C_3N_4 nanobelts	10 vol% TEOA	3	46.3	300 W Xe lamp λ ≥ 400 nm	10.1016/j.apcatb.2019.117931
8	P-doped g-C_3N_4	10 vol% TEOA	1		300 W Xe lamp λ ≥ 420 nm	10.1016/j.apcatb.2018.10.044
9	P-doped carbon nitride nanotubes	10 vol% TEOA	3	145.8	300 W Xe lamp	10.1016/j.carbon.2023.03.038
10	U-CN-N	10 vol% TEOA	3	130	300 W Xe lamp	10.1016/j.apcatb.2017.06.067
11	3D g-C_3N_4 NR	10 vol% TEOA	1	600	300 W Xenon lamp	10.1016/j.apcatb.2019.117761
12	PCNS-2	10 Vol% TEOA	1	366	300 W Xenon lamp	10.1021/acssuschemeng.7b00559
13	PCN-S	10 Vol% TEOA	1	318	300 W Xenon lamp	10.1016/j.cjche.2020.06.037
14	CN-SP	20 mL Methanol	1	570	300 W Xenon lamp	10.1016/j.apcatb.2017.07.022
15	**PCN210**	**10 vol% TEOA**	**1.5**	**1089**	**White LED**	**Present Study**

Table S7: Comparison of the Apparent Quantum Yield

S.No	Photocatalyst	Pt (wt%)	Wavelength (nm)	Scavenger	AQE (%)	Reference
1	BP NSs	5	500	10 Vol% TEOA	0.5	10.1016/j.ijhydene.2019.06.087
2	P-doped g-C_3N_4	3	435	10 Vol% TEOA	0.7	10.1039/C4TA05292G
3	CNS-Pt-B	1	420	10 Vol% TEOA	0.6	10.1021/acssuschemeng.8b01835
4	Sr-TiO_2	1 mg Pt/mL	470	10 Vol% TEOA	0.67	10.1016/j.jphotochem.2020.112705
5	PtSA-CN6201	1.72	420	10 Vol% TEOA	0.17	10.1016/j.nanoen.2018.11.033
6	*sg*-CN-PTZ	2	415	10 Vol% TEOA	0.32	10.1002/cssc.202002500
			440	10 Vol% TEOA	0.25	10.1002/cssc.202002500
7	RuCat/Pt-g-C_3N_4	1	400	100 mM MBA	0.28	10.1016/j.apcatb.2017.11.072
8	**CN-210P**	**1.5**	**450**	**10 Vol% TEOA**	**1.6**	**This work**
9	**CN-210P**	**1.5**	**520**	**10 vol % TEOA**	**1.01**	**This work**
10	**CN-210P**	**1.5**	**630**	**10 vol % TEOA**	**0.16**	**This work**
11	**CN-210P**	**1.5**	**450**	**20 mM BAOH**	**0.34**	**This work**

Table S8: Summary of photoluminescence (PL) average decay time (τ) determined from time-resolved PL (TRPL) measurements.

Sample	τ_1 (ns)	τ_2 (ns)	A_1 (%)	A_2 (%)	R^2	Average decay time (τ) (ns)
CN	3.29	15.5	56.00	43.99	0.998	8.65
CN-105P	2.36	10.6	62.72	37.27	0.997	5.44
CN-210P	1.92	7.65	57.52	42.47	0.999	4.35
CN-315P	1.56	8.73	68.73	31.26	0.997	4.01

References

1. S. Ding, J. B. Gabriel Filho, T. Peppel, S. Haida, J. Rabeah, N. Steinfeldt and J. Strunk, *Sustain. Energy Fuels*, 2023, **7**, 4396–4400.